A&A 652, A123 (2021)
https://doi.org/10.1051/0004-6361/202141032

Astronomy & Astrophysics

The slope of the low-energy spectrum of prompt gamma-ray burst emission

M. Toffano[1], G. Ghirlanda[2,3], L. Nava[2,8,9], G. Ghisellini[2], M. E. Ravasio[4], and G. Oganesyan[5,6,7]

[1] Universitá degli Studi dell'Insubria, Via Valleggio 11, 22100 Como, Italy
e-mail: mattia.toffano@inaf.it
[2] INAF – Osservatorio Astronomico di Brera, Via E. Bianchi 46, 23807 Merate, Italy
[3] INFN – Sezione di Milano-Bicocca, Piazza della Scienza 3, 20126 Milano, Italy
[4] Universitá degli Studi di Milano-Bicocca, Dip. di Fisica "G. Occhialini", Piazza della Scienza 3, 20126 Milano, Italy
[5] Gran Sasso Science Institute, Viale F. Crispi 7, 67100 L'Aquila (AQ), Italy
[6] INFN – Laboratori Nazionali del Gran Sasso, 67100 L'Aquila (AQ), Italy
[7] INAF – Osservatorio Astronomico d'Abruzzo, Via M. Maggini snc, 64100 Teramo, Italy
[8] INFN – Sezione di Trieste, via Valerio 2, 34149 Trieste, Italy
[9] Institute for Fundamental Physics of the Universe (IFPU), 34151 Trieste, Italy

Received 9 April 2021 / Accepted 1 June 2021

ABSTRACT

The prompt emission spectra from gamma-ray bursts (GRBs) are often fitted with the empirical "Band" function, namely two smoothly connected power laws. The typical slope of the low-energy (sub-MeV) power law is $\alpha_{\rm Band} \simeq -1$. In a small fraction of long GRBs this power law splits into two components such that the spectrum presents, in addition to the typical ∼MeV νF_ν peak, a break at the order of a few keV or hundreds of keV. The typical power law slopes below and above the break are −0.6 and −1.5, respectively. If the break is a common feature, the value of $\alpha_{\rm Band}$ could be an "average" of the spectral slopes below and above the break in GRBs fitted with Band function. We analyze the spectra of 27 (9) bright long (short) GRBs detected by the *Fermi* satellite, finding a low-energy break between 80 keV and 280 keV in 12 long GRBs, but in none of the short events. Through spectral simulations we show that if the break is moved closer (farther) to the peak energy, a harder (softer) $\alpha_{\rm Band}$ is found by fitting the simulated spectra with the Band function. The hard average slope $\alpha_{\rm Band} \simeq -0.38$ found in short GRBs suggests that the break is close to the peak energy. We show that for 15 long GRBs best fitted by the Band function only, the break could be present but not identifiable in the *Fermi*/GBM spectrum, because either at low energies, close to the detector limit ($\alpha_{\rm Band} \lesssim -1$), or in the proximity of the energy peak ($\alpha_{\rm Band} \gtrsim -1$). A spectrum with two breaks could be typical of GRB prompt emission, albeit hard to identify with current detectors. Instrumental design such as that conceived for the THESEUS space mission, extending from 0.3 keV to several MeV and featuring a larger effective area with respect to *Fermi*/GBM, could reveal a larger fraction of GRBs with spectral energy breaks.

Key words. gamma rays: general

1. Introduction

The prompt emission spectra of gamma-ray bursts (GRBs) are usually described by empirical functions. The most commonly used is the Band function (Band et al. 1993), which consists of two smoothly connected power laws $N(E) \propto E^{\alpha_{\rm Band}}$ and $N(E) \propto E^{\beta_{\rm Band}}$ describing the photon spectrum at low and high energies, respectively. Spectral studies of long GRBs (LGRBs; i.e., observed duration >2 s; Kouveliotou et al. 1993) detected by the Burst And Transient Source Experiment (BATSE) on board the *Compton* Gamma Ray Observatory (CGRO) showed that, on average, $\alpha_{\rm Band} \sim -1$, $\beta_{\rm Band} \sim -2.3$, and the $E^2N(E)$ spectral energy distribution peaks at $E_{\rm peak} \sim 300$ keV (Kaneko et al. 2006). Similar results were obtained by spectral studies of GRBs detected by the *Fermi* Gamma-ray Burst Monitor (GBM; Gruber et al. 2014; von Kienlin et al. 2020; Nava et al. 2011a) and the *Beppo*SAX Gamma-Ray Burst Monitor (GRBM; Frontera et al. 2009). Short GRBs (SGRBs) have on average a harder $\alpha_{\rm Band} \sim -0.6$ (Ghirlanda et al. 2004, 2009) and a larger observed peak energy[1].

[1] Accounting for the different redshift distributions, the peak energy of short and long GRBs become similar (Ghirlanda et al. 2015; Nava et al. 2012).

Recently, in a sizable fraction of LGRBs detected simultaneously by the Burst Alert Telescope (BAT) and the X-Ray Telescope (XRT) aboard the *Neil Gehrels Swift* Observatory (hereafter *Swift*), and in the brightest GRBs detected by *Fermi*/GBM, it was found that (a) a low-energy spectral break is present, between ∼1 and a few hundred keV, and that (b) the slopes of the power law below and above this break are consistent with the values expected from synchrotron emission (Oganesyan et al. 2017, 2018; Ravasio et al. 2018, 2019). The consistency of GRB spectra with synchrotron emission was also demonstrated using direct fits with a synchrotron model (Oganesyan et al. 2019; Chand et al. 2019; Burgess et al. 2020; Ronchi et al. 2020). The interpretation of these results within the leptonic synchrotron scenario is quite challenging, requiring a small magnetic field (∼10 G) and a large dissipation radius (10^{16-17} cm) (Kumar & McMahon 2008; Daigne 2011; Beniamini & Piran 2013; Geng et al. 2018; Oganesyan et al. 2019; Ronchi et al. 2020). Synchrotron emission from protons has been proposed as a possible solution (Ghisellini et al. 2020), but the matter is still under debate (Florou et al. 2021).

While the presence of a low-energy spectral break has been identified in a subsample of GRBs, a sizable fraction of GRB spectra are well fitted by single break functions where the break

energy corresponds to $E_{\rm peak}$. If the presence of an additional break located at lower energies is a common feature in GRB spectra, its non-detection could be due to several factors. For spectra with a low signal-to-noise ratio (S/N) the identification of a change in slope might be difficult. Also, if the break is either close to the peak energy or below the low-energy edge of the instrument sensitivity, a spectral fit would be unable to identify the break. Burgess et al. (2015) studied how the Band function fits spectra simulated assuming a synchrotron or a synchrotron plus black-body model.

In this work, we investigate the possibility that the low-energy spectral break is a common feature in GRB spectra, and that the average spectral index $\alpha_{\rm Band} \sim -1$ is an average value between the two power-law segments below and above the break energy. To this aim we analyze bright long and short GRBs detected by *Fermi* (Sects. 2 and 3) in search for statistically significant evidence of the low-energy spectral break. Through spectral simulations we study how the value of $\alpha_{\rm Band}$ becomes harder (softer) by moving the break closer to (farther from) the peak energy (Sect. 4). We derive (Sect. 4.2) limits on the possible location of the break energy in GRBs whose spectrum is best fitted by the Band function (i.e., with no evidence of a break). We discuss and summarize our results in Sect. 5.

2. The sample

To perform our investigation, we first need to characterize the low-energy part of GRB spectra, searching for possible spectral breaks like those recently reported in a number of events. To this aim, we select GRBs detected by the GBM (8 keV–40 MeV; Meegan et al. 2009) and apply selection criteria that maximize the probability of (i) performing reliable spectral analysis and (ii) identifying the presence of a spectral break at low energies, well distinguished from the spectral peak energy. This can be achieved by selecting GRBs with large fluence and large $E_{\rm peak}$ values, as they are more likely to display the low-energy break $E_{\rm break}$ within the energy range of the GBM, given that their typical separation is $E_{\rm break}/E_{\rm peak} \sim 0.1$ (Ravasio et al. 2019).

For these reasons, from the online *Fermi* catalog[2], which contains 2669 GRBs up to April 2020, we select LGRBs[3] with fluence $>10^{-4}$ erg cm^{-2} (integrated over the 10–1000 keV energy range) and observed peak energy $E_{\rm peak} > 300$ keV, and SGRBs with fluence $>5\times10^{-6}$ erg cm^{-2} and $E_{\rm peak} > 300$ keV. This selection is based on the values of fluence and peak energy reported in the catalog and corresponding to the fit of the time-integrated spectrum with the Band function. We excluded GRB 090902B because the presence of a power-law component (in addition to a multi–temperature black body; Ryde et al. 2010; Liu & Wang 2011; Pe'er et al. 2012) hampers the identification of the spectral break at low energies. Our selection results in 27 long and 9 short GRBs.

3. Spectral analysis

The *Fermi*/GBM consists of 12 sodium iodide (NaI – 8–1000 keV) and 2 bismuth germanate (BGO – 0.2–40 MeV) detectors. For each burst, we analyzed the data from two NaI detectors and one BGO, selected as those with the smallest GRB position angle with respect to the detector normal.

We used the public tool `gtburst`[4] to retrieve spectral CSPEC data from the *Fermi* Data Server[5]. We extract the time-integrated spectrum over the time interval T_{90} reported in the *Fermi* catalog. In the cases of GRB 130427A and GRB 160625B, which have a multi-peaked, long-duration light curve, we consider the brightest portion of the light curve by selecting the time intervals 3.0–15 s and 188–210 s, respectively[6]. We estimated the background spectrum by selecting two time intervals before and after (far from) the GRB emission episode. The latest detector response matrices for each event were obtained through `gtburst`.

Standard energy selections[7] for the analyzed spectra were applied (8–900 keV for NaIs and 0.3–40 MeV for BGO) and the 30–40 keV range was excluded to avoid contamination of inaccurate modeling of the iodine K-edge line at 33.17 keV in the response files. The spectral data for the two NaI and one BGO were fitted together accounting for an inter-calibration constant parameter.

The extracted spectra were analyzed with `XSPEC`[8] (v12.10.1). All spectra were fitted with two different spectral models:

– the Band function (Band et al. 1993), often used to fit GRB spectra (Preece et al. 1998; Kaneko et al. 2006; Ghirlanda et al. 2002; Nava et al. 2011b; Sakamoto et al. 2011; Gruber et al. 2014; Yu et al. 2016; Lien et al. 2016; Goldstein et al. 2012; Frontera et al. 2000):

$$N(E) \propto \begin{cases} E^{\alpha} e^{-E/E_0}, & \text{if } E \le (\alpha-\beta)E_0 \\ [(\alpha-\beta)E_0]^{(\alpha-\beta)} E^{\beta} e^{(\beta-\alpha)}, & \text{if } E > (\alpha-\beta)E_0, \end{cases} \quad (1)$$

where α and β are the photon indices of the power laws below and above, respectively, the e-folding energy E_0. Here, $N(E)$ is in units of ph cm^{-2} s^{-1} keV^{-1}. For $\beta < -2 < \alpha$, the spectrum in the $E^2N(E)$ representation peaks at $E_{\rm peak} = E_0(\alpha+2)$.

– the double smoothly broken power-law function (2SBPL hereafter, Ravasio et al. 2018)

$$N(E) \propto E_{\rm break}^{\alpha_1} \cdot \left\{ \left[\left(\frac{E}{E_{\rm break}} \right)^{-\alpha_1 n_1} + \left(\frac{E}{E_{\rm break}} \right)^{-\alpha_2 n_1} \right]^{n_2/n_1} + \left(\frac{E}{E_j} \right)^{-\beta n_2} \cdot \left[\left(\frac{E_j}{E_{\rm break}} \right)^{-\alpha_1 n_1} + \left(\frac{E_j}{E_{\rm break}} \right)^{-\alpha_2 n_1} \right]^{n_2/n_1} \right\}^{-1/n_2} \quad (2)$$

where

$$E_j = E_{\rm peak} \cdot \left(-\frac{\alpha_2 + 2}{\beta + 2} \right)^{1/[(\beta-\alpha_2)n_2]}, \quad (3)$$

and $E_{\rm peak}$ and $E_{\rm break}$ are the peak of the νF_ν spectrum and the break energy, respectively. The parameters α_1 and α_2 are the power-law indices below and above the break energy, and β is the power-law index above the peak energy. The parameters n_1 and n_2 set the sharpness of the curvature around $E_{\rm break}$ and $E_{\rm peak}$, respectively. Following Ravasio et al. (2019), we assumed $n_1 = n_2 = 2$.

[2] https://heasarc.gsfc.nasa.gov/W3Browse/fermi/fermigbrst.html
[3] GRBs are classified into long and short based on the values of T_{90} reported in the *Fermi* online catalog, with a separation at 2 s.
[4] https://fermi.gsfc.nasa.gov/ssc/data/analysis/scitools/gtburst.html
[5] https://fermi.gsfc.nasa.gov/ssc/data/access/
[6] A detailed analysis of the first peak (0–2.5 s) of GRB 130427A has been performed in Preece et al. (2014).
[7] https://fermi.gsfc.nasa.gov/ssc/data/analysis/scitools/
[8] https://heasarc.gsfc.nasa.gov/xanadu/xspec/

Table 1. Results of the fits for GRBs best fitted by a 2SBPL.

Name	$\alpha_{\rm Band}$	$E_{\rm peak,Band}$	$\beta_{\rm Band}$	$\alpha_{1,\rm 2SBPL}$	$\alpha_{2,\rm 2SBPL}$	$E_{\rm break,2SBPL}$	$E_{\rm peak,2SBPL}$	$\beta_{\rm 2SBPL}$	$\chi^2_{r,\rm Band}$	$\chi^2_{r,\rm 2SBPL}$	$\rm AIC_{Band}$	$\rm AIC_{2SBPL}$
100724(029)	$-0.71^{+0.01}_{-0.01}$	339^{+12}_{-12}	$-2.09^{+0.03}_{-0.03}$	$-0.80^{+0.01}_{-0.02}$	$-1.90^{+0.05}$	168^{+23}_{-13}	345^{+380}_{-226}	$-2.35^{+0.10}_{0.11}$	0.99	0.92	463	441
100918(863)	$-0.74^{+0.05}_{-0.04}$	406^{+51}_{-49}	$-2.47^{+0.12}_{-0.17}$	$-0.74^{+0.07}_{-0.05}$	< -1.77	146^{+20}_{-34}	523^{+159}_{-124}	$-3.17^{+0.36}_{-0.5}$	0.94	0.89	221	213
130427(324)	$-0.66^{+0.01}_{-0.01}$	$852^{+6.7}_{-6.7}$	$-3.27^{+0.03}_{-0.03}$	$-0.63^{+0.01}_{-0.01}$	$-1.67^{+0.03}_{-0.03}$	224^{+10}_{-10}	992^{+12}_{-12}	$-3.7^{+0.04}_{-0.04}$	6.01	2.83	942	812
131014(215)	$-0.21^{+0.01}_{-0.01}$	306^{+4}_{-4}	$-2.72^{+0.02}_{-0.02}$	$-0.33^{+0.01}_{-0.01}$	$-1.8^{+0.04}_{-0.04}$	124^{+6}_{-6}	386^{+14}_{-15}	$-3.48^{+0.09}_{-0.10}$	2.17	1.35	642	620
131028(076)	$-0.66^{+0.01}_{-0.01}$	860^{+28}_{-25}	$-3.34^{+0.14}_{-0.18}$	$-0.65^{+0.02}_{-0.02}$	$-1.68^{+0.07}_{-0.07}$	249^{+23}_{-23}	991^{+64}_{-56}	$-3.74^{+0.17}_{-0.2}$	1.26	1.14	438	401
150510(139)	$-1.01^{+0.01}_{-0.01}$	1172^{+118}_{-52}	< -3.88	$-0.86^{+0.05}_{-0.04}$	$-1.52^{+0.10}_{-0.11}$	173^{+42}_{-35}	1776^{+221}_{197}	$-4.90^{+0.61}_{-0.89}$	1.07	0.97	374	342
160509(374)	$-0.89^{+0.04}_{-0.04}$	468^{+60}_{-53}	$-2.73^{+0.13}_{-0.14}$	$-0.63^{+0.10}_{-0.12}$	$-1.66^{+0.08}_{-0.07}$	80^{+22}_{-17}	2071^{+635}_{-545}	$-2.82^{+0.14}_{-0.12}$	1.01	0.95	484	460
160625(945)	$-0.54^{+0.01}_{-0.01}$	362^{+6}_{-6}	$-2.26^{+0.01}_{-0.01}$	$-0.55^{+0.01}_{-0.01}$	$-1.71^{+0.02}_{-0.02}$	120^{+3}_{-3}	684^{+21}_{-20}	$-2.75^{+0.03}_{-0.03}$	4.73	1.64	1607	568
160821(857)	$-0.95^{+0.01}_{-0.01}$	836^{+17}_{-17}	$-2.22^{+0.02}_{-0.02}$	$-0.86^{+0.04}_{-0.03}$	$-1.56^{+0.08}_{-0.09}$	150^{+23}_{-24}	1362^{+74}_{-66}	$-2.6^{+0.11}_{-0.09}$	2.06	1.53	932	699
170409(112)	$-0.79^{+0.01}_{-0.01}$	839^{+27}_{-25}	$-2.58^{+0.04}_{-0.05}$	$-0.79^{+0.01}_{-0.01}$	$-1.81^{+0.04}_{-0.04}$	278^{+15}_{-15}	1292^{+118}_{-105}	$-3.48^{+0.19}_{-0.16}$	1.53	1.27	700	588
171227(000)	$-0.81^{+0.01}_{-0.01}$	737^{+33}_{-31}	$-2.53^{+0.04}_{-0.04}$	$-0.63^{+0.05}_{-0.05}$	$-1.49^{+0.07}_{-0.07}$	112^{+24}_{-22}	968^{+70}_{-59}	$-2.86^{+0.09}_{-0.07}$	1.37	0.95	320	227
180720(598)	$-1.04^{+0.01}_{-0.01}$	472^{+15}_{-14}	$-2.37^{+0.05}_{-0.06}$	$0.97^{+0.05}_{-0.04}$	$1.78^{+0.06}_{-0.05}$	121^{+15}_{-17}	951^{+135}_{-106}	$-2.99^{+0.16}_{-0.13}$	1.87	1.49	853	685

Notes. The parameters obtained by fitting a Band function are also shown for comparison. Analyzed GRBs are listed in Col. 1 (in parenthesis, the trigger name according to the *Fermi* catalog). The parameters concerning the Band function (Cols. 2–4) and the 2SBPL function (Cols. 5–9) are defined in Eqs. (1) and (2), respectively. The reduced χ^2 statistics (χ^2_r) and the AIC for each fit are shown in Cols. 10–13. Both errors and upper limits are calculated at 1σ confidence level. Energies are expressed in keV.

In the following, in order to distinguish the spectral parameters of these two fitting functions, we refer to the photon indices of the Band function as $\alpha_{\rm Band}$ and $\beta_{\rm Band}$, the photon indices of the 2SBPL below the peak energy as $\alpha_{1,\rm 2SBPL}$ and $\alpha_{2,\rm 2SBPL}$, and the photon index of the 2SBPL above the peak energy as $\beta_{\rm 2SBPL}$.

The large number of counts of the extracted spectra allow us to fit the spectra and search for the best-fit parameters by minimizing the χ^2 statistics. We adopt the Akaike information criterion (AIC – Akaike 1974) to compare the fits obtained with the 2SBPL and Band functions and choose the best one. We recall that $\rm AIC = 2k - 2\ln(\hat{L})$, where k is the number of free parameters in the model and $\hat{L}$ is the maximum value of the likelihood function L obtained by varying the free parameters. For Gaussian-distributed variables $\chi^2 \propto -2\ln(L)$. If $\Delta\rm AIC = AIC_{Band} - AIC_{2SBPL} \geq 6$, the Band fit has $\lesssim$5% probability of describing the observed spectrum better than the 2SBPL function (Akaike 1974): in such a case, we consider the 2SBPL a better fit and thus consider the presence of a break as statistically significant at the 95% confidence level.

3.1. Fit results: best-fit model

The fit results for LGRBs are reported in Tables 1 and 2. The fit results for SGRBs are shown in Table 3. The errors on the parameters represent the 1σ confidence[9].

We find that:

– of the 27 LGRBs, 12 have a low-energy break, that is, their spectra are best fitted by the 2SBPL function ($\Delta\rm AIC \geq 6$). The spectral parameters are reported in Table 1;
– the remaining 15 LGRBs are well fitted by the Band function and, according to the AIC criterion, there is no improvement using the 2SBPL function. Their spectral parameters are reported in Table 2;
– all SGRBs are well fitted by the Band function. In six SGRBs we could only derive an upper limit on $\beta_{\rm Band}$, indicating that also a cutoff power-law function could be a good fit to the spectra (see e.g., Ghirlanda et al. 2004).

In the LGRB 160509A, we find a well-constrained $E_{\rm break} \simeq 80$ keV but the peak energy of the 2SBPL is undetermined by fitting the GBM data. Only in this case did we exploit the LAT Low Energy (LLE) data to better constrain the high-energy index β and thus $E_{\rm peak}$. With `gtburst` we extracted the time-integrated spectrum from the LLE data[10] and performed a joint GBM-LLE spectral fit over the 10 keV–300 MeV energy range. Assuming an intercalibration normalization factor between LAT-LLE and NaI detectors of 1, we obtained an estimate of $E_{\rm peak} \simeq 2071$ keV for GRB 160509A (Table 1).

3.2. Fit results: spectral indices below E_{peak}

Figure 1 (top panel) shows the distribution of the spectral index $\alpha_{\rm Band}$ for the entire sample. The blue histogram corresponds to LGRBs without the break and the green dashed histogram is for SGRBs (all without a break). For comparison we also show the distribution of $\alpha_{\rm Band}$ for the 12 LGRBs whose spectrum is better fitted by the 2SBPL.

In the bottom panel of Fig. 1 we show the distributions of the indices $\alpha_{1,\rm 2SBPL}$ (red) and $\alpha_{2,\rm 2SBPL}$ (violet) for the 12 LGRBs best fitted by the 2SBPL (i.e., with an identified low-energy spectral break). The characteristic values (mean, median, and 1σ dispersion) of the distributions in Fig. 1 are reported in Tables 4 and 5.

From the comparison of the distributions shown in Fig. 1 we find that:

1. SGRBs (green dashed histogram) have a harder spectral slope $\alpha_{\rm Band}$ than LGRBs without a break (blue histogram). A Kolmogorov-Smirnov (KS) test[11] among the two distributions returns a p-value of 0.004, rejecting the null hypothesis that these GRBs are drawn from the same underlying distribution. This is consistent with previous studies (Ghirlanda et al. 2004, 2009);
2. the value of $\alpha_{\rm Band}$ for LGRBs with a break (orange histogram in Fig. 1, top panel) is on average harder (see Table 4) than the value for LGRBs with no break (blue histogram). However, the two distributions are indistinguishable (a KS test

[9] Through the `error` method built in `XSPEC`.

[10] https://heasarc.gsfc.nasa.gov/W3Browse/fermi/fermille.html

[11] For all the statistical tests we have set the significance level at 0.05, i.e. we accept the null hypothesis if $p > 0.05$.

Table 2. Results of the fits for GRBs best fitted by a Band function.

Name	$\alpha_{\rm Band}$	$E_{\rm peak,Band}$	$\beta_{\rm Band}$	$\chi^2_{r,\rm Band}$	$\rm AIC_{Band}$
090323(002)	$-1.08^{+0.03}_{-0.02}$	340^{+34}_{-30}	$-2.47^{+0.17}_{-0.33}$	0.90	420
090926(181)	$-0.70^{+0.01}_{-0.01}$	291^{+5}_{-5}	$-2.64^{+0.04}_{-0.05}$	1.50	861
100414(097)	$-0.49^{+0.02}_{-0.02}$	561^{+21}_{-19}	< -4.7	1.14	518
101123(952)	$-0.95^{+0.02}_{-0.02}$	448^{+45}_{-40}	$-2.31^{+0.11}_{-0.15}$	0.88	307
120526(303)	$-0.81^{+0.03}_{-0.03}$	752^{+68}_{-62}	$-3.35^{+0.33}_{-0.62}$	0.90	215
120624(933)	$-0.95^{+0.03}_{-0.03}$	580^{+75}_{-65}	$-2.30^{+0.12}_{-0.18}$	1.00	464
120711(115)	$-0.93^{+0.01}_{-0.01}$	1108^{+65}_{-79}	$-3.26^{+0.15}_{-0.20}$	0.94	223
130306(991)	$-0.81^{+0.21}_{-0.17}$	211^{+64}_{-51}	< -2.78	0.59	263
130504(978)	$-1.22^{+0.02}_{-0.02}$	656^{+86}_{-74}	$-2.46^{+0.13}_{-0.17}$	0.97	229
130606(497)	$-1.05^{+0.01}_{-0.01}$	329^{+16}_{-14}	$-2.11^{+0.02}_{-0.02}$	1.52	692
140206(275)	$-1.33^{+0.02}_{-0.02}$	309^{+33}_{-29}	$-2.19^{+0.09}_{-0.11}$	0.98	432
160905(471)	$-0.86^{+0.02}_{-0.02}$	905^{+71}_{-61}	$-3.10^{+0.29}_{-0.75}$	1.16	534
170210(116)	$-1.08^{+0.02}_{-0.02}$	500^{+54}_{-47}	$-2.36^{+0.12}_{-0.17}$	0.91	320
170214(649)	$-0.82^{+0.03}_{-0.03}$	370^{+25}_{-22}	$-2.48^{+0.10}_{-0.12}$	1.15	532
170527(480)	$-1.03^{+0.02}_{-0.02}$	823^{+56}_{-52}	< -4.21	1.09	502

Notes. Analyzed GRBs are listed in Col. 1 (in parenthesis, the trigger name according to the *Fermi* catalog). The parameters regarding the Band function (Cols. 2–4) are defined in Eq. (1). The reduced χ^2 statistics (χ^2_r) and the AIC for each fit are shown in Cols. 5–6. Both errors and upper limits are calculated at 1σ confidence level. Energies are expressed in keV.

Table 3. Results of the fits performed using the Band function for the SGRBs in our sample.

Name	$\alpha_{\rm Band}$	$E_{\rm peak,Band}$	$\beta_{\rm Band}$	$\chi^2_{r,\rm Band}$	$\rm AIC_{Band}$
090227(772)	$-0.48^{+0.19}_{-0.17}$	1830^{+108}_{-136}	$-3.05^{+0.19}_{-0.26}$	1.01	336
090228(204)	$-0.5^{+0.02}_{-0.02}$	621^{+50}_{-48}	< -4.41	1.12	482
111222(619)	$-0.28^{+0.08}_{-0.07}$	616^{+64}_{-58}	< -4.04	1.21	358
130504(314)	$-0.28^{+0.04}_{-0.05}$	990^{+75}_{-72}	< -4.52	1.04	337
130701(761)	$-0.47^{+0.06}_{-0.06}$	869^{+107}_{-98}	< -4.56	0.98	443
150819(440)	$-1.04^{+0.03}_{-0.03}$	400^{+45}_{-22}	< -4.09	0.95	314
170127(067)	$+0.3^{+0.14}_{-0.13}$	768^{+64}_{-62}	$-4.05^{+0.51}_{-1.01}$	1.00	176
170206(453)	$-0.12^{+0.05}_{-0.05}$	274^{+17}_{-17}	$-2.76^{+0.10}_{-0.11}$	1.00	442
170222(209)	$-0.56^{+0.08}_{-0.07}$	700^{+100}_{-89}	< -4.41	0.89	312

Notes. Analyzed GRBs are listed in Col. 1 (in parenthesis, the trigger name according to the *Fermi* catalog). The parameters regarding the Band function (Cols. 2–4) are defined in Eq. (1). The reduced χ^2 statistics (χ^2_r) and the AIC for each fit are shown in Cols. 5–6. Both errors and upper limits are calculated at 1σ confidence level. Energies are expressed in keV.

between the orange and blue distributions has a chance probability $p = 0.08$);

3. the distributions of $\alpha_{1,\rm 2SBPL}$ and $\alpha_{2,\rm 2SBPL}$ (red and violet histograms in Fig. 1, bottom panel) are peaked at -0.71 and -1.71, not far from the typical values $-2/3$ and $-3/2$ expected for synchrotron spectrum from marginally fast cooling electrons;
4. LGRBs without a break have an $\alpha_{\rm Band}$ distribution that is slightly softer than $\alpha_{1,\rm 2SBPL}$ but harder than $\alpha_{2,\rm 2SBPL}$ (cf. the blue histogram in the top panel with the red and violet histogram in the bottom panel of Fig. 1 respectively). This might suggest that when the spectral data are not sufficient to constrain and identify a spectral break, the Band function returns a value of the low-energy index that is an average between the index $\alpha_{1,\rm 2SBPL}$ and $\alpha_{2,\rm 2SBPL}$. This possibility is investigated with simulations in the following section;
5. the distribution of $\alpha_{\rm Band}$ of SGRBs (green) is similar to the $\alpha_{1,\rm 2SBPL}$ distribution of LGRBs with a break: a KS test between the two returns $p = 0.16$. This suggests that the power-law segment $\alpha_{2,\rm 2SBPL}$ separating $E_{\rm break}$ from $E_{\rm peak}$ is not present in SGRBs, i.e., $E_{\rm break} \sim E_{\rm peak}$.

4. Origin of the value $\alpha_{\rm Band} \sim -1$

The spectral analysis presented in this paper confirms the presence of two classes of LGRBs: those requiring two power-law segments ($\alpha_{1,\rm 2SBPL}$ and $\alpha_{2,\rm 2SBPL}$) to describe the spectrum at energies $E < E_{\rm peak}$, and those for which this part of the spectrum is well described by a single power law ($\alpha_{\rm Band}$). As the values of $\alpha_{\rm Band}$ are typically softer than $\alpha_{1,\rm 2SBPL}$ but harder than $\alpha_{2,\rm 2SBPL}$, we investigate the possibility that spectra best fitted by Band are hiding a spectral break that is difficult to identify with a

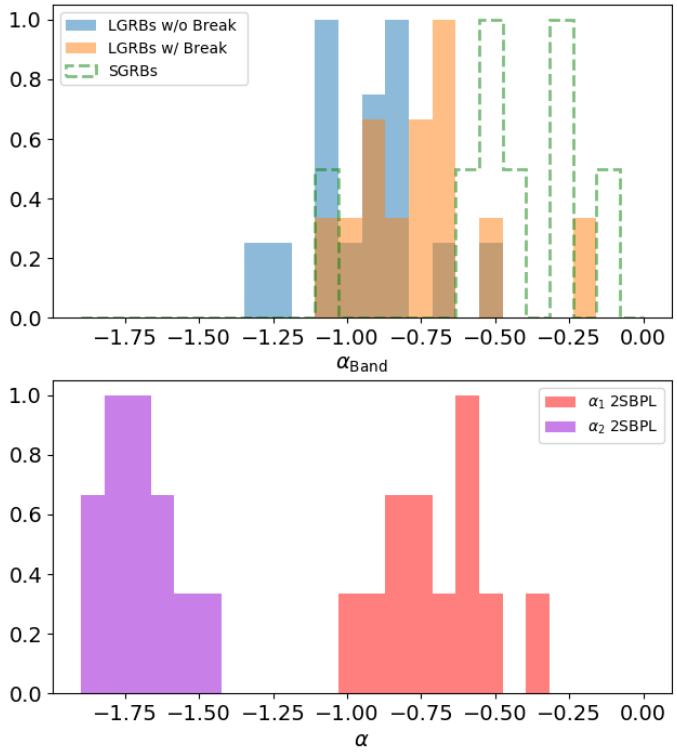

Fig. 1. *Top*: distributions of $\alpha_{\rm Band}$ for SGRBs (green) and for both LGRBs with and without the low-energy spectral break (orange and blue histogram). *Bottom*: distributions of $\alpha_{1,2\rm SBPL}$ and $\alpha_{2,2\rm SBPL}$ of the 12 LGRBs best fitted by the 2SBPL (i.e., with the low-energy spectral break). Distributions are normalized to their peak values.

certain statistical significance due to the lack of enough signal at low energies, and/or to the proximity of $E_{\rm break}$ to $E_{\rm peak}$, and/or to the proximity of $E_{\rm break}$ to the low-energy edge of the GBM sensitivity. If this is correct, we would expect to see a dependence of $\alpha_{\rm Band}$ on the values of $E_{\rm break}$ and $E_{\rm peak}$ and on their separation. Specifically, we expect that when the underlying spectrum has a break, the fit with the Band function will return a hard $\alpha_{\rm Band} \sim \alpha_{1,2\rm SBPL}$ when $E_{\rm break} \sim E_{\rm peak}$, and, conversely, a soft $\alpha_{\rm Band} \sim \alpha_{2,2\rm SBPL}$ when $E_{\rm break} \ll E_{\rm peak}$.

A strong correlation is not expected, as the value of $\alpha_{\rm Band}$ should depend not only on the ratio $R_E = E_{\rm break}/E_{\rm peak}$, but also on the absolute value of $E_{\rm peak}$ (or, equivalently, $E_{\rm break}$), and also on the specific values of $\alpha_{1,2\rm SBPL}$ and $\alpha_{2,2\rm SBPL}$. To better investigate this effect and its presence in the spectra, we performed a set of simulations that are described in the following sections.

4.1. Band function response to a spectral break

In this first section we investigate how the presence of a spectral break generally affects the results of a fit performed using the Band function. We simulate GRB prompt spectra with input model 2SBPL, keeping fixed all the parameters and varying solely $E_{\rm break}$. The adopted input parameters are $\alpha_{1,2\rm SBPL} = -0.65$, $\alpha_{2,2\rm SBPL} = -1.67$, $E_{\rm peak} = 1000\,$keV, $\beta_{2\rm SBPL} = -2.5$. These input values have been chosen in order to reproduce a typical LGRB of our sample (see the fit results in Sect. 3). For these simulations, we use the GBM background and response matrix files from one of the GRBs in our sample. We verified that choosing different background and response matrix files belonging to any other GRB in our sample does not affect the simulation results.

Table 4. Characteristic values (mean, median and 68% interval) of the distributions of $\alpha_{\rm Band}$ shown in the top panel of Fig. 1.

GRB type	N	$\langle\alpha_{\rm Band}\rangle$	$\tilde{\alpha}_{\rm Band}$	68% interval
LGRB w/ break	12	−0.75	−0.76	[−0.90, −0.57]
LGRB w/o break	15	−0.94	−0.95	[−1.08, −0.80]
SGRB	9	−0.38	−0.47	[−1.03, 0.3]

Notes. The number of GRBs in each sample is reported in Col. 2.

Table 5. Characteristic values (mean, median and 68% interval) of the distributions of $\alpha_{1,2\rm SBPL}$ and $\alpha_{2,2\rm SBPL}$ shown in the bottom panel of Fig. 1 for the 12 LGRBs best fitted with the 2SBPL.

Index	$\langle\alpha_i\rangle$	$\tilde{\alpha}_i$	68% interval
$\alpha_{1,2\rm SBPL}$	−0.71	−0.70	[−0.86, −0.60]
$\alpha_{2,2\rm SBPL}$	−1.71	−1.69	[−1.82, −1.62]

Each simulated spectrum is then fitted with the input model (a 2SBPL with parameters free to vary) and also with a Band function. For each value of $E_{\rm break}$, we repeated the simulation 200 times, obtaining (for each parameter and for the reduced chi-square) a distribution of values. From these distributions we extracted the mean value and its 68% confidence interval. Figure 2 shows the parameters returned by the Band fits as a function of the position of the energy break. This exercise is repeated for two different cases, with a rather high average S/N[12] (∼21, left-hand panel) and a S/N ratio that is approximately a factor 10 lower (∼2.7, right-hand panel). They represent simulated spectra of a GRB with a fluence of $\sim 3.5 \cdot 10^{-4}\,$erg cm^{-2} and $\sim 3.5 \cdot 10^{-5}\,$erg cm^{-2}, respectively. The input parameters used for the 2SBPL function used for the simulations ($\alpha_{1,2\rm SBPL}$, $\alpha_{2,2\rm SBPL}$, $E_{\rm peak}$, $\beta_{2\rm SBPL}$) are marked by dashed horizontal lines. We distinguish the best-fitting model according to our criterion based on the AIC (in Fig. 2, diamonds: 2SBPL, circles: Band).

The values of $\alpha_{\rm Band}$ obtained by fitting the simulated spectra with the Band function (orange symbols in the top panel) correlate with $E_{\rm break}$: a low value of $E_{\rm break}$ makes $\alpha_{\rm Band} \approx \alpha_{2,2\rm SBPL}$. On the other hand, as $E_{\rm break}$ increases (and approaches $E_{\rm peak}$ which in this example is 1 MeV) $\alpha_{\rm Band} \approx \alpha_{1,2\rm SBPL}$. In between, the value of $\alpha_{\rm Band}$ is an average of $\alpha_{1,2\rm SBPL}$ and $\alpha_{2,2\rm SBPL}$, depending on the position of $E_{\rm break}$. Given the presence of only a single break in the Band function (i.e., $E_{\rm peak,Band}$) the other parameters ($\beta_{\rm Band}$ and $E_{\rm peak,Band}$) also depend on the position of the break: $\beta_{\rm Band}$ (blue symbols) always assumes softer values compared to the input one, unless $E_{\rm break} \sim E_{\rm peak}$. $E_{\rm peak,Band}$ (green symbols) is an average of $E_{\rm break}$ and $E_{\rm peak}$ of the 2SBPL function and approaches the input value when $E_{\rm break}$ is very low or when $E_{\rm break} \sim E_{\rm peak}$.

These results hold for both S/Ns. The main difference is in the uncertainties on the best fit parameters (larger for the case with lower S/N) and, most notably, on the behavior of the χ^2_r. In the case with lower S/N, the χ^2_r of the Band fit is always acceptable (∼1), regardless of the value of $E_{\rm break}$. This shows that, even though the input spectrum has a spectral break and this break falls within the GBM energy range, identification of the break is not possible in a spectrum with a relatively low S/N,

[12] Calculated as $(s - b)/\sqrt{b}$, where s and b are the source and background estimated counts, respectively (see e.g., Dereli-Bégué et al. 2020).

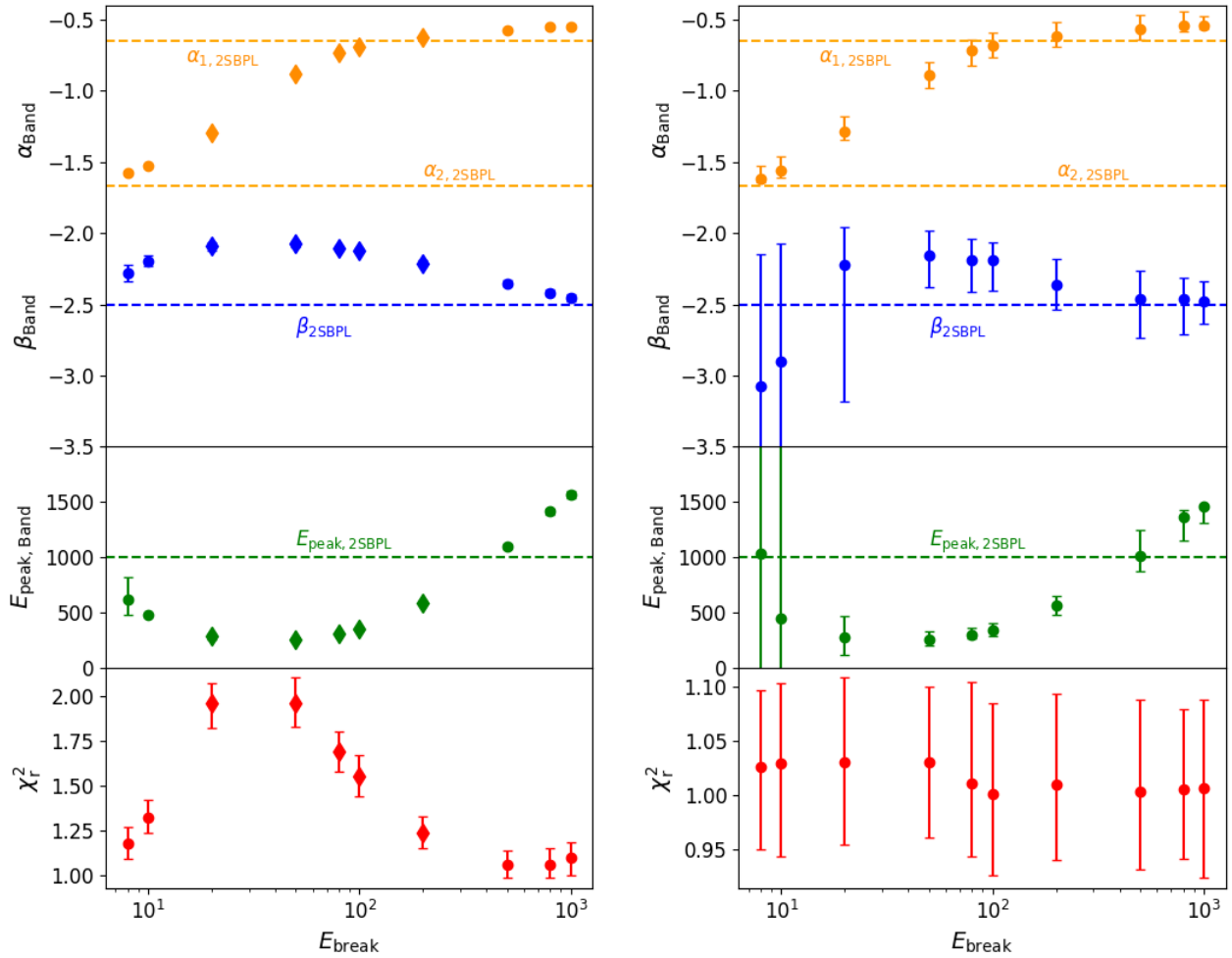

Fig. 2. Band function parameters as a function of the position of the energy break $E_{\rm break}$ of the 2SBPL function. Each plot shows the parameters of the Band function fitted to a series of spectra simulated assuming the 2SBPL function whose parameter values are marked by the horizontal dashed lines. *Top*: low-energy slope $\alpha_{\rm Band}$ (orange symbols) and high-energy slope $\beta_{\rm Band}$ (blue symbols). *Middle*: energy peak $E_{\rm peak,Band}$ (green symbols). *Bottom*: fit χ^2_r (red symbols). *Left*: spectrum characterized by a $S/N \sim 21$ (fluence $\sim 3.5 \cdot 10^{-4}$ erg cm^{-2}). *Right*: spectrum characterized by $S/N \sim 2.7$ (fluence $\sim 3.5 \cdot 10^{-5}$ erg cm^{-2}). Data are represented as circles when the best-fitting model is Band and as diamonds when the best-fitting model is 2SBPL.

and the best-fit model is a Band function. We note that a fluence of $3.5 \cdot 10^{-5}$ erg cm^{-2} or less is representative of the majority of LGRBs detected by *Fermi*/GBM. If the S/N is increased by a factor of ten (left-hand panel), the χ^2_r of the fit with the Band function depends on $E_{\rm break}$: only when the break is at the very-low-energy end of the GBM spectral range ($E_{\rm break} \lesssim 10$ keV) or close to $E_{\rm peak}$ ($E_{\rm break} \gtrsim 500$ keV) does the fit with the Band function return an acceptable χ^2_r. Despite the high S/N, in such cases the break is hardly identifiable (ΔAIC < 6).

Finally, we notice that even when the Band function returns an adequate fit, (i.e., when $E_{\rm break} \lesssim 10$ keV or $E_{\rm break} \sim E_{\rm peak}$) the resulting values of $\alpha_{\rm Band}$, $\beta_{\rm Band}$, and $E_{\rm peak,Band}$ might largely deviate from the values of the input spectrum.

4.2. Spectral simulations: $R_E - \alpha_{Band}$ trend

In order to further investigate the $R_E - \alpha_{\rm Band}$ trend, we focus first on the 12 LGRBs analyzed in this work that have a spectral break $E_{\rm break}$. In Fig. 3 we show (orange symbols) their ratio $R_E = E_{\rm break}/E_{\rm peak}$ (from the fits of the 2SBPL) versus $\alpha_{\rm Band}$ (from the fit of the same spectrum with the Band function). LGRBs with a break are located in the range $R_E \in [0.04, 0.5]$ and, if their spectra are fitted with the Band function, the resulting $\alpha_{\rm Band}$ is in the range $\alpha_{\rm Band} \in [-1.1, -0.2]$. A broad trend in the $R_E - \alpha_{\rm Band}$ plane appears among the points. The Pearson correlation coefficient is 0.56 and the associated chance probability value $p = 0.05$.

For each of these GRBs, we simulate[13] spectra with the 2SBPL function with parameter values fixed to the best-fit values (reported in Table 1) except for $E_{\rm break}$, which we vary between $0.01E_{\rm peak}$ and $E_{\rm peak}$. For each GRB, we used the corresponding GBM background and response matrix files for the corresponding simulations. Simulated spectra were renormalized in order to maintain the energy-integrated flux of the real spectrum constant while moving $E_{\rm break}$. Low values of R_E place the break below the GBM low-energy threshold, i.e., 8 keV, in those GRBs with $E_{\rm peak,2SBPL} < 800$ keV. We then refit the simulated spectra with the Band function and derive $\alpha_{\rm Band}$. The simulation of each spectrum is repeated 200 times to build the distribution of $\alpha_{\rm Band}$ and estimate its mean value and 68% confidence interval.

In Fig. 3 we show, for each of the 12 LGRBs, the corresponding $\alpha_{\rm Band}$ returned by the fit with the Band function for each input value of R_E (orange dashed line). These curves show that

[13] Spectral simulation performed within `XSPEC` with the `fakeit` tool.

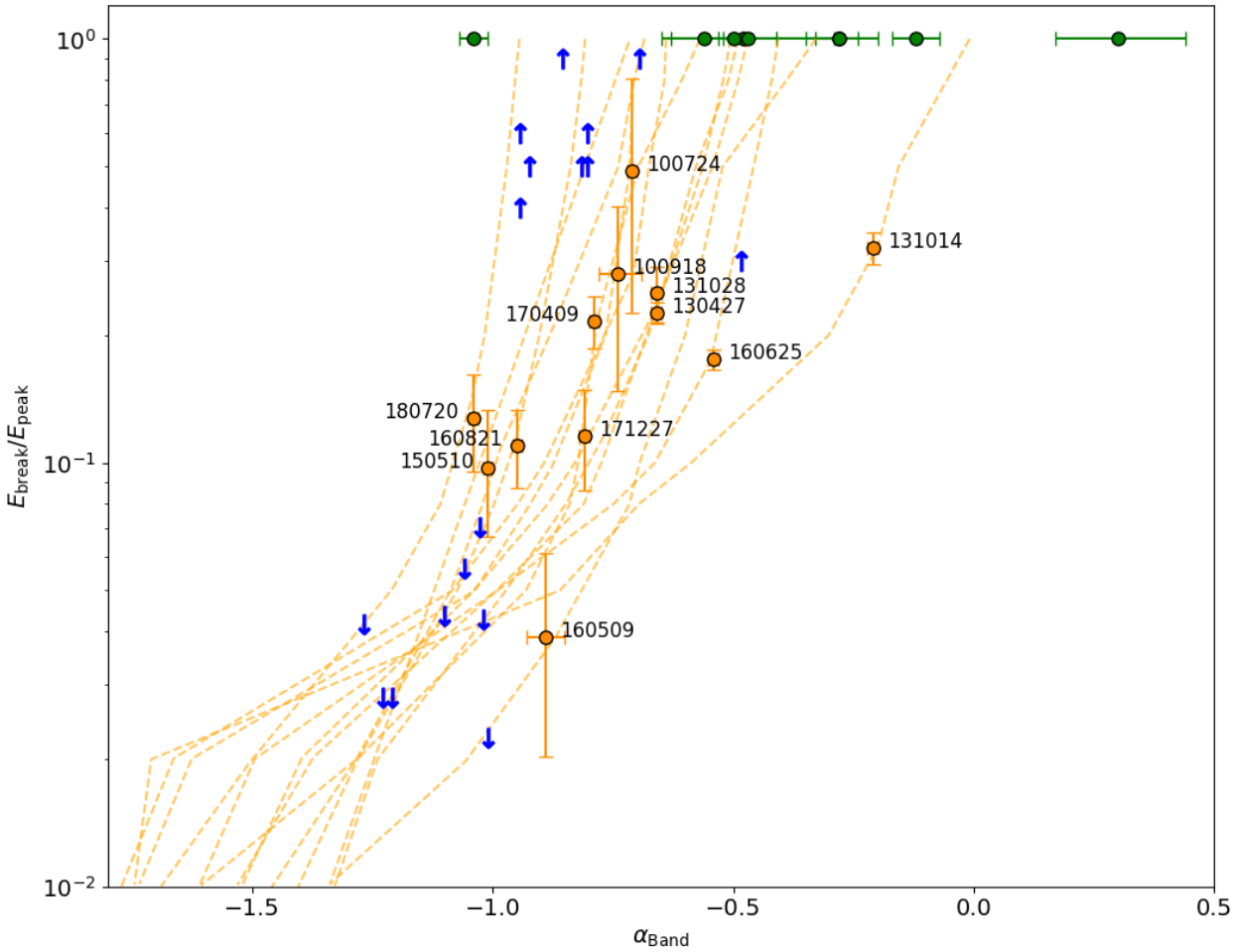

Fig. 3. 12 LGRBs best fitted by a 2SBPL (Table 1) shown with orange symbols. Their value of $R_E = E_{\rm break}/E_{\rm peak}$ is shown vs. the value of the index $\alpha_{\rm Band}$ that is obtained by fitting their spectrum with a Band function. SGRBs (whose spectrum is always best fitted by the Band function) are represented here assuming that, if the underlying spectrum were 2SBPL, it would be expected to have $E_{\rm break} \sim E_{\rm peak}$ (green symbols). The orange dashed lines show the results of simulations (see Sect. 4.2); blue arrows represent the upper and lower limits on R_E for the 15 LGRBs whose spectra are best fitted by Band (see Sect. 4.3).

$\alpha_{\rm Band}$ depends on the relative position between break and peak energy, with small ratios resulting in soft spectra and large ratios resulting in harder spectra, as expected. These simulations show that the value of $\alpha_{\rm Band}$ is a "weighted" mean of the $\alpha_{1,\rm 2SBPL}$ and $\alpha_{2,\rm 2SBPL}$ slopes. Moreover, different curves show similar trends, showing that the different values of $E_{\rm peak}$ and input $\alpha_{1,\rm 2SBPL}$ and $\alpha_{2,\rm 2SBPL}$ are responsible for the dispersion in the plane. The dispersion of the curves is similar to the dispersion in the real data.

From the tracks of the orange dashed lines shown in Fig. 3 we can speculate that, when the best-fit model is a Band function, values of $\alpha_{\rm Band}$ harder than ~ -1.0 could be consistent with the presence of an $E_{\rm break}$ in the proximity (i.e., until one order of magnitude lower) of $E_{\rm peak}$, while values softer than ~ -1.0 could indicate the presence of $E_{\rm break}$ far from (i.e., more than one order of magnitude lower than) $E_{\rm peak}$. This possibility is investigated in the following section, through spectral simulations.

4.3. Spectral simulations: origin of the spectra without a low-energy break

Fifteen LGRBs in our sample do not show the presence of a low-energy spectral break. Through spectral simulations, we now propose to investigate whether or not it is still possible for these GRBs to have a low-energy break, even though the best-fit model is a simple Band function. The simulation now assumes that also in these 15 GRBs the spectrum has the shape of the 2SBPL function and infers constraints on its parameters by requiring that the fit with the Band function is not only acceptable but also preferred over a 2SBPL, and returns as best-fit values the same values as the real spectrum.

Based on the trend found between R_E and $\alpha_{\rm Band}$, we would expect that if the spectrum is intrinsically a 2SBPL and $E_{\rm break}$ lies at low energies, the Band function could adequately fit the simulated spectrum and result in $\alpha_{\rm Band} \sim \alpha_{2,\rm 2SBPL}$. Similarly, if the spectrum is intrinsically a 2SBPL and $E_{\rm break}$ lies close to $E_{\rm peak}$, the Band function could return $\alpha_{\rm Band} \sim \alpha_{1,\rm 2SBPL}$. For each burst, the spectra simulated with the 2SBPL function maintain the same fluence of the real GRB.

We repeat the simulations for different values of the 2SBPL parameters. In particular:

- $\alpha_{1,\rm 2SBPL}$ is sampled uniformly within the range $[-0.3, -1.05]$ with steps of 0.03;
- $\alpha_{2,\rm 2SBPL}$ is sampled uniformly in the interval $\in [-1.1, -1.9]$ with steps of 0.03;
- $E_{\rm break}$ is sampled between 2 keV and the energy peak with steps of 2 keV;
- $\beta_{\rm 2SBPL}$ is fixed to the value obtained from the fit with the Band function.

Table 6. Constraints on $\alpha_{2,2SBPL}$ and maximum E_{break} (in keV) for GRBs with soft α_{Band} that did not show an energy break in their time-integrated spectrum.

Name	$\alpha_{2,2SBPL}$ Range	$E_{break,Max}$
090323(002)	[−1.48, −1.18]	30
130504(978)	[−1.42, −1.28]	12
130606(497)	[−1.24, −1.12]	12
140206(275)	[−1.60, −1.36]	18
170210(116)	[−1.37, −1.14]	24
170527(480)	[−1.34, −1.15]	24

Table 7. Constraints on $\alpha_{1,2SBPL}$ and minimum E_{break} (in keV) for GRBs with hard α_{Band} that did not show an energy break in their time-integrated spectrum.

Name	$\alpha_{1,2SBPL}$ Range	$E_{break,Min}$
090926(181)	[−0.83, −0.80]	220
100414(097)	[−0.68, −0.54]	126
101123(952)	[−1.02, −0.94]	182
120526(303)	[−0.90, −0.83]	372
120624(933)	[−1.05, −0.93]	320
120711(115)	−0.95	440
130306(991)	[−0.98, −0.72]	86
160905(471)	[−0.90, −0.84]	572
170214(649)	[−0.92, −0.86]	158

For each combination of parameters, we simulate ten spectra. We assume the background and response matrix files of each GRB for these simulations. These spectra are then refitted with both the 2SBPL and Band functions. From the built parameter distributions we derive the mean values and 68% confidence interval. Once we refit the spectrum with a Band function we accept the simulation if the Band fit satisfies the following conditions:

- it is statistically equivalent to the fit with the 2SBPL, i.e., $\Delta AIC < 6$;
- its α_{Band} and β_{Band} are consistent, within 1σ, with the values inferred from the real spectrum;
- its E_{peak} is consistent, within 3σ, with the value inferred from the real spectrum.

For each of the 15 LGRBs that do not explicitly show a break, we find a significant number of parameter combinations for which the 2SBPL functions were able to satisfactorily reproduce the real spectrum.

In particular, for all these LGRBs we are able to set either a plausible maximum or minimum value for E_{break} and constrain either $\alpha_{2,2SBPL}$ or $\alpha_{1,2SBPL}$ in an interval. These are represented with the blue arrows in Fig. 3. The limits for E_{break} and the low-energy slope intervals are listed in Tables 6 and 7.

5. Discussion and conclusions

The prompt emission spectra of long GRBs are often fitted with the Band function, two power laws smoothly joined at the νF_ν peak. The low-energy index (below the peak energy E_{peak}) $\alpha_{Band} \sim -1$ has been used as an argument against the interpretation of the prompt emission as synchrotron (see e.g., Preece et al. 1998; Frontera et al. 2000; Ghirlanda et al. 2002). Recently, different groups identified a break, E_{break}, at low energies below E_{peak} (Oganesyan et al. 2017, 2018, 2019; Ravasio et al. 2018, 2019) paving the way towards a solution to the long-standing issue on the nature of the prompt emission process (see e.g., Daigne 2011; Uhm & Zhang 2014; Bošnjak et al. 2009; Ghisellini & Celotti 1999; Rees & Mészáros 1994; Sari et al. 1996, 1998).

According to these latter works, the prompt emission spectra of the brightest GRBs can be described with three power laws (with indexes $\alpha_{1,2SBPL}$ below E_{break}, $\alpha_{2,2SBPL}$ between E_{break} and E_{peak} and β above it) smoothly joined at the two breaks, namely E_{break} and E_{peak}.

If the spectrum is a 2SBPL, our simulations described in Sect. 4.1 show that when E_{break} is close to E_{peak} or below the low-energy threshold (E_{min}) of the instrument, the Band function gives $\alpha_{Band} \sim \alpha_{2,2SBPL}$ and $\alpha_{Band} \sim \alpha_{1,2SBPL}$, respectively. Values of $\alpha_{Band} \sim -1$ correspond to E_{break} between E_{min} and E_{peak}. Through the spectral analysis of a sample of GRBs selected with different criteria, Burgess et al. (2020) find that, when $E_{break} \lesssim E_{peak}$, the values of α_{Band} are distributed approximately $\in [-1.7, -0.5]$. We argue that, if the break is a common feature of GRB spectra, the value of α_{Band} is a proxy of its position with respect to E_{peak}.

This hypothesis is verified through the spectral analysis of a sample of 27 long and 9 short GRBs selected from within the *Fermi* sample with large fluence and large E_{peak} (Sect. 2) in order to ease the search for E_{break}, if present. In 12 out of the 27 long GRBs, we find E_{break} (i.e., the 2SBPL fits the data better than Band). Through spectral simulations, using these events as templates, we find that if the break is moved within the range delimited by E_{peak} and E_{min}, the fit with Band results in a softer (if E_{break} departs from E_{peak}) or harder (if E_{break} approaches E_{peak}) low-energy index α_{Band} (dashed orange lines in Fig. 3). At the extremes, the values of $\alpha_{1,2SBPL}$ and $\alpha_{2,2SBPL}$ are found. Indeed, none of the SGRBs analyzed have a break, but they all have a relatively hard α_{Band} which we suggest corresponds to E_{break} lying close to E_{peak}. Through dedicated spectral simulations (Sect. 4.3) we show that the 15 LGRBs best fitted by the Band function only (i.e., apparently without a break) could instead have a break close to E_{peak}, corresponding to $\alpha_{Band} > -1$ (upward arrows in Fig. 3), or close to E_{min} if $\alpha_{Band} < -1$ (downward arrows in Fig. 3).

Our analysis suggests that the low-energy break could be a more common feature than is suggested by direct spectral analysis. Indeed, the identification of the break in the spectra of GRBs detected by *Fermi* or *Swift*, currently only possible for a limited number of events (shown in Fig. 4), is hampered by (1) the separation of E_{break} from E_{peak} and (2) the spectral signal-to-noise ratio. We show (right panel of Fig. 2) that a burst with a typical fluence (e.g., $5 \cdot 10^{-6}$ erg cm^{-2}) detected by *Fermi*/GBM can be fitted by Band even if it has an additional break. Taken together, these effects explain why we were not able to find E_{break} in approximately half of the selected GRBs but, through simulations, were able to set an upper or lower limit on its possible value.

With the currently available instruments, *Swift* and *Fermi*, it was possible to find E_{break} in a limited number of GRBs and with E_{break} at X-ray (∼few keV) and γ–ray (∼tens – hundreds keV) energies (Fig. 4). A few values of E_{break} between 10 and 100 keV are found.

Our results (Fig. 1 – bottom panel) show that the distributions of $\alpha_{1,2SBPL}$ and $\alpha_{2,2SBPL}$ are close to but slightly softer than the values predicted by synchrotron emission in the moderate fast cooling regime (Daigne 2011), that is, −3/2 and −2/3, respectively. This is partly thanks to our fits with the 2SBPL function rather than with the synchrotron model (see e.g., Burgess et al. 2015, 2020) and to the fact that we analyze time-integrated spectra to exploit the highest S/N in search of

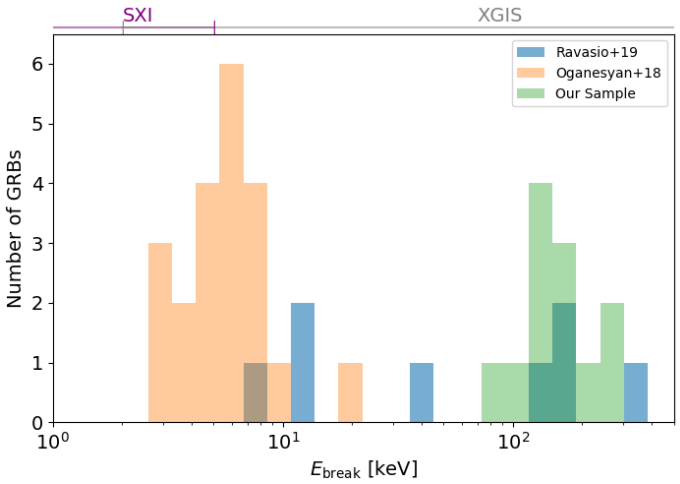

Fig. 4. Energy distribution of the spectral breaks identified in prompt spectra of GRBs, from the results of Oganesyan et al. (2018), Ravasio et al. (2019), and this work. The horizontal lines indicate the observational energy range of the instrumentation aboard THESEUS.

$E_{\rm break}$. Time-resolved spectral analyses, indeed, often find harder spectral slopes (Nava et al. 2011a; Acuner & Ryde 2017) and, as shown by Ravasio et al. (2019), the distributions of $\alpha_{1,\rm 2SBPL}$ and $\alpha_{2,\rm 2SBPL}$ are closer to the typical synchrotron values.

With the Transient High-Energy Sky and Early Universe Surveyor (THESEUS) mission (Amati et al. 2018, 2021) proposed to ESA within the M5-class selection call, we expect that the spectral break will be detected in a larger fraction of events (Ghirlanda et al. 2021). The large effective area and the wide energy range covered by the two instruments on board THESEUS, namely the Soft X-ray Imager (SXI, 0.3–5 keV) and X-Gamma rays Imaging Spectrometer (XGIS, 2 keV–few MeV), will provide highly statistically significant prompt emission spectra from which $E_{\rm break}$ will be measured over a wider fluence range than is currently possible.

Acknowledgements. G. O. acknowledges financial contribution from the agreement ASI-INAF n.2017-14-H.0. G. Ghirlanda acknowledges the Premiale project FIGARO 1.05.06.13 and INAF-PRIN 1.05.01.88.06.

References

Acuner, Z., & Ryde, F. 2017, MNRAS, 475, 1708
Akaike, H. 1974, IEEE Trans. Autom. Control, 19, 716
Amati, L., O'Brien, P., Götz, D., et al. 2018, Adv. Space Res., 62, 191
Amati, L., O'Brien, P. T., Götz, D., et al. 2021, Exp. Astron., submitted, [arXiv: 2104.09531]
Band, D., Matteson, J., Ford, L., et al. 1993, ApJ, 413, 281
Beniamini, P., & Piran, T. 2013, ApJ, 769, 69
Bošnjak, Ž., Daigne, F., & Dubus, G. 2009, A&A, 498, 677
Burgess, J. M., Ryde, F., & Yu, H.-F. 2015, MNRAS, 451, 1511
Burgess, J. M., Bégué, D., Greiner, J., et al. 2020, Nat. Astron., 4, 174
Chand, V., Chattopadhyay, T., Oganesyan, G., et al. 2019, ApJ, 874, 70
Daigne, F., Bošnjak, Ž., & Dubus, G. 2011, A&A, 526, A110
Dereli-Bégué, H., Pe'er, A., & Ryde, F. 2020, ApJ, 897, 145
Florou, I., Petropoulou, M., & Mastichiadis, A. 2021, MNRAS, 505, 1367
Frontera, F., Amati, L., Costa, E., et al. 2000, ApJS, 127, 59
Frontera, F., Guidorzi, C., Montanari, E., et al. 2009, ApJS, 180, 192
Geng, J.-J., Huang, Y.-F., Wu, X.-F., Zhang, B., & Zong, H.-S. 2018, ApJS, 234, 3
Ghirlanda, G., Celotti, A., & Ghisellini, G. 2002, A&A, 393, 409
Ghirlanda, G., Ghisellini, G., & Celotti, A. 2004, A&A, 422, L55
Ghirlanda, G., Nava, L., Ghisellini, G., Celotti, A., & Firmani, C. 2009, A&A, 496, 585
Ghirlanda, G., Bernardini, M. G., Calderone, G., & D'Avanzo, P. 2015, J. High Energy Astrophys., 7, 81
Ghirlanda, G., Salvaterra, R., Toffano, M., et al. 2021, Exp. Astron., in press, [arXiv:2104.10448]
Ghisellini, G., & Celotti, A. 1999, ApJ, 511, L93
Ghisellini, G., Ghirlanda, G., Oganesyan, G., et al. 2020, A&A, 636, A82
Goldstein, A., Burgess, J. M., Preece, R. D., et al. 2012, ApJS, 199, 19
Gruber, D., Goldstein, A., Weller von Ahlefeld, V., et al. 2014, ApJS, 211, 12
Kaneko, Y., Preece, R. D., Briggs, M. S., Paciesas, W. S., & Meegan, C. 2006, ApJS, 166, 298
Kouveliotou, C., Meegan, C. A., Fishman, G. J., et al. 1993, ApJ, 413, L101
Kumar, P., & McMahon, E. 2008, MNRAS, 384, 33
Lien, A., Sakamoto, T., Barthelmy, S. D., et al. 2016, ApJ, 829, 7
Liu, R.-Y., & Wang, X.-Y. 2011, ApJ, 730, 1
Meegan, C., Lichti, G., Bhat, P. N., et al. 2009, ApJ, 702, 791
Nava, L., Ghirlanda, G., Ghisellini, G., & Celotti, A. 2011a, A&A, 530, A21
Nava, L., Ghirlanda, G., Ghisellini, G., & Celotti, A. 2011b, MNRAS, 415, 3153
Nava, L., Salvaterra, R., Ghirlanda, G., et al. 2012, MNRAS, 421, 1256
Oganesyan, G., Nava, L., Ghirlanda, G., & Celotti, A. 2017, ApJ, 846, 137
Oganesyan, G., Nava, L., Ghirlanda, G., & Celotti, A. 2018, A&A, 616, A138
Oganesyan, G., Nava, L., Ghirlanda, G., Melandri, A., & Celotti, A. 2019, A&A, 628, A59
Pe'er, A., Zhang, B.-B., Ryde, F., et al. 2012, MNRAS, 420, 468
Preece, R. D., Briggs, M. S., Mallozzi, R. S., et al. 1998, ApJ, 506, L23
Preece, R., Burgess, J. M., von Kienlin, A., et al. 2014, Science, 343, 51
Ravasio, M. E., Oganesyan, G., Ghirlanda, G., et al. 2018, A&A, 613, A16
Ravasio, M. E., Ghirlanda, G., Nava, L., & Ghisellini, G. 2019, A&A, 625, A60
Rees, M. J., & Mészáros, P. 1994, ApJ, 430, L93
Ronchi, M., Fumagalli, F., Ravasio, M. E., et al. 2020, A&A, 636, A55
Ryde, F., Axelsson, M., Zhang, B. B., et al. 2010, ApJ, 709, L172
Sakamoto, T., Barthelmy, S. D., Baumgartner, W. H., et al. 2011, ApJS, 195, 2
Sari, R., Narayan, R., & Piran, T. 1996, ApJ, 473, 204
Sari, R., Piran, T., & Narayan, R. 1998, ApJ, 497, L17
Uhm, Z. L., & Zhang, B. 2014, Nat. Phys., 10, 351
von Kienlin, A., Meegan, C. A., Paciesas, W. S., et al. 2020, ApJ, 893, 46
Yu, H.-F., Preece, R. D., Greiner, J., et al. 2016, A&A, 588, A135